Master's Thesis of Engineering

Kinetic Simulation of Gas Breakdown in Narrow Holes

좁은 홀에서 발생하는 기체 방전의 동역학 시뮬레이션 연구

August 2023

Graduate School of Engineering
Seoul National University
Energy Systems Engineering Major

Sung Hyun Son

Kinetic Simulation of Gas Breakdown in Narrow Holes

Kyoung-Jae Chung

Submitting a master's thesis of
Engineering

August 2023

Graduate School of Engineering
Seoul National University
Energy Systems Engineering Major

Sung Hyun Son

Confirming the master's thesis written by
Sung Hyun Son
August 2023

Chair Yong-Su Na (Seal)
Vice Chair Kyoung-Jae Chung (Seal)
Examiner June Young Kim (Seal)

Abstract

Gas breakdown, which has been studied throughout history, is the foundational knowledge in plasma physics. However, understanding complex discharges in realistic situations remains a challenging task. Particularly, comprehending gas breakdown in narrow hole structures, especially in the presence of background plasma, is crucial for mitigating unintended arcing in semiconductor fabrication devices. In this study, we conducted controlled experiments and combined them with two-dimensional plasma kinetic simulations to comprehensively investigate the fundamental physics of gas breakdown in high aspect ratio hole structures. One of the key findings is that in narrow structures, the major source of secondary electrons shifts from ion-induced emission at the cathode to electron-induced emission from the walls. Furthermore, by simulating the presence of background plasma near the narrow holes, we observed a significant decrease in breakdown voltage, leading to the occurrence of unintended discharges, which was consistent with experimental observations. Through kinetic simulations, we demonstrated that the initial electron avalanche process caused by the influx of charged particles from the background plasma contributes to the accumulation of local space charge and the distortion of the electric field inside the hole. Since the ionization coefficient is nonlinearly proportional to the electric field strength, this distorted electric field profile leads to enhanced electron multiplication even at lower applied voltages, resulting in a reduced breakdown voltage.

Keyword: Gas breakdown, Kinetic simulation, Particle-In-Cell, Background plasma, Space-charge, Plasma processing

Student Number: 2020-24257

Contents

List of Figures

Chapter 1. Introduction

The physics of gas breakdown provides a fundamental understanding of various gas discharges. Starting from Townsend's theory of the gas breakdown, numerous studies attempted to explore the gas breakdown physics in various situations. The Paschen curve, evaluated from the Townsend discharge model, has successfully scaled the characteristics of breakdown in different situations based on the product of the background gas pressure and the inter-electrode distance [1-6]. While this model describes breakdown voltages for simple discharges, many experimental and theoretical studies have demonstrated that the gas breakdown voltage in the realistic situations cannot be solely explained by classical theory [7-9]. After that, various works have focused on investigating sophisticated factors such as complex electrode shapes, surface materials, and driving voltage types, which have shown significant effects on gas breakdown [10-61]. Scholars have conducted extensive experimental and theoretical investigations into non-trivial phenomena regarding the gas breakdown. For instance, Lisovskiy et al. studied gas breakdown in cylinders with various aspect ratios, presenting an analytic model that explains the breakdown voltage of a thin tube could not be explained by classical theory. They suggested the modification of the Paschen curve for long tube discharges primarily affected by radial electron loss, which is signified by the aspect ratio increment [22-28]. From another view, several studies have also examined micro-gap discharges,

revealing that the ion-induced secondary electron emission, which is typically the major source of the secondary electrons is no longer dominant. They experimentally suggested the transition from ion-induced secondary electron emission to electric-field-induced electron emissions as the dominant source [29-46]. Loveless and Garner incorporated this change into the classical Townsend model, resulting in a universal theory that covers the range from micro- to macro-scale gas discharges [46]. Furthermore, the effects of secondary electron emission, caused not only by ion bombardment but also by fast neutrals and energetic electrons on the in direct-current (DC) breakdown or the electrode in radio-frequency (RF) breakdown have been investigated [47-61]. All these works stand that the Townsend's model of gas discharge is very elegant yet not incompatible for specific situations.

Meanwhile, as the demand on plasma applications is rapidly increasing in the wide industrial field from the semiconductor fabrication to the plasma medicine, the physics of plasma discharge is getting more attention. Understanding the criteria for discharge ignition must be secured for diversified applications, such as operating various types of plasma sources. Contribution from the previous works have enabled us to comprehend the basic underlying physics of plasma discharges, but there are still many challenging discharges that require further research. Narrow hole breakdown occurring during plasma-assisted process exemplifies the challenge. A *narrow hole* is a thin cylinder which contains a lateral electrode rather than planar electrodes in a tube geometry. They exist in the numerous of plasma source chambers, in the form gas injection holes and engineering gaps, as commonly and inevitably.

Unintended discharge from this structure is known as a major phenomenon causing physical damage to the chamber and generation of impurities that adversely affect the stability. Until now, efforts have focused on changing structures of the hole empirically, while a fundamental solution has not been presented due to the lack of understanding the fundamental gas breakdown physics [68]. As mentioned, despite that some studies studied the unique properties of a *tube* discharge, study on the gas breakdown in a narrow hole is still lacking. In specific, one should dig in the dynamics of secondary electron emission in a narrow hole discharge since the previous works on the tube discharge suggested that the electron loss to the radial wall gets more importance.

Studying the physics of a narrow hole discharge would not only widen the physical understanding of gas discharges, but also contribute preventing unintended narrow hole breakdowns in various plasma sources. To do so, one also should account the effect from the existence of the background plasma into the investigation. Since all the previous studies share a common initial condition in which the background is a neutral gas, they are not compatible for examining the effect of the background plasma on the gas discharges. Hence, narrow hole discharges in various realistic plasma sources, shown in Figure 1.1, requires a different point of view. This kind of discharge becomes more impact, since it exemplifies numerous discharges ignited from gas-filled gaps facing a background plasma, which is a basic form of breakdown encountered in various situations. Mechanical gaps in plasma-facing

components or plasma guns attached to fusion devices could be also explained by the discharge physics of a gap facing a stand-alone plasma [62-67].

This thesis represents a significant contribution to the understanding of narrow hole breakdown, which is essential for various technological applications. The research is a comprehensive investigation of the topic, utilizing a combination of experiments and multi-dimensional kinetic simulations. The structure of the thesis is organized, with each chapter addressing specific aspects of the research. Chapter 2 provides an in-depth theoretical background on gas breakdown, which is essential for understanding the subsequent chapters. This section helps to establish a strong foundation for the study and provides a context for the reader to understand the experimental and simulation results presented in the following chapters. Chapter 3 is a detailed description of the research methods utilized in the study. The chapter provides an overview of the experimental setups and kinetic simulation techniques employed to study the gas breakdown in narrow holes. This section is essential as it enables the reader to comprehend the data presented in the subsequent chapters. Chapter 4 delves into the fundamental mechanisms of gas breakdown in narrow holes through kinetic simulations. The chapter provides insights into the key breakdown processes, α and γ, and assesses the impact of secondary electron emission on gap breakdown. This section presents the findings of the simulation in a clear and concise manner, providing a better understanding of the factors affecting narrow hole breakdown. In Chapter 5, the role of background plasma in narrow hole breakdown is emphasized. This section presents a crucial aspect of the study, as

background plasma plays a vital role in the breakdown process. The chapter provides a thorough analysis of the data, which is essential for the reader to understand the impact of background plasma on narrow hole breakdown. Finally, Chapter 6 presents the conclusion of the study. This section summarizes the key findings and provides insights into future research directions. Overall, the thesis provides a significant contribution to the understanding of narrow hole breakdown, and the well-structured organization of the thesis enhances the readability and comprehension of the research.

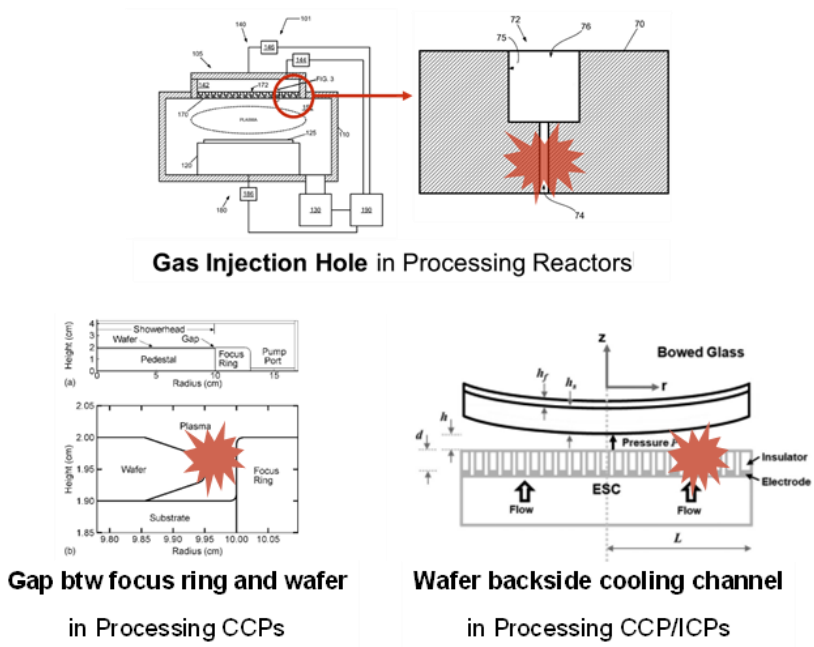

Figure 1.1 Various sites where narrow hole breakdown can occur in processing reactors. Gas injection holes, mechanical gap between the focus ring and wafer, and backside cooling channel of a wafer.

Chapter 2. Background theory

2.1. Townsend's model of gas discharge

Gas breakdown from a vacuum space is usually initiated by the ionization phenomenon caused by cosmic rays within the reactor's internal space or by seed electrons naturally generated on the electrode surface through the photoelectric effect, which are then accelerated by the steady-state DC voltage applied to the electrodes. The accelerated seed electrons undergo ionizing reactions with the gas inside the reactor, generating ions. These ions are accelerated towards the cathode, which is negatively charged, causing secondary electron emission upon impact. The generated secondary electrons are further accelerated by the electric field and, following the same mechanism as the seed electrons, generate more ions. This chain reaction of electron and ion multiplication is referred to as an avalanche. The voltage at which a sufficient electric field is established between the electrodes to sustain the plasma is called the breakdown voltage or insulation breakdown voltage. Figure 2.1 provides a summarized illustration of the overall mechanism of DC glow discharge. Townsend first quantitatively modeled those gas breakdowns, or gas discharges, suggesting two major factors governing the physical phenomenon named as α and γ. As mentioned in Chapter 1, this simple model is not accountable for realistic discharges, yet it provides some fundamental knowledges of gas discharges.

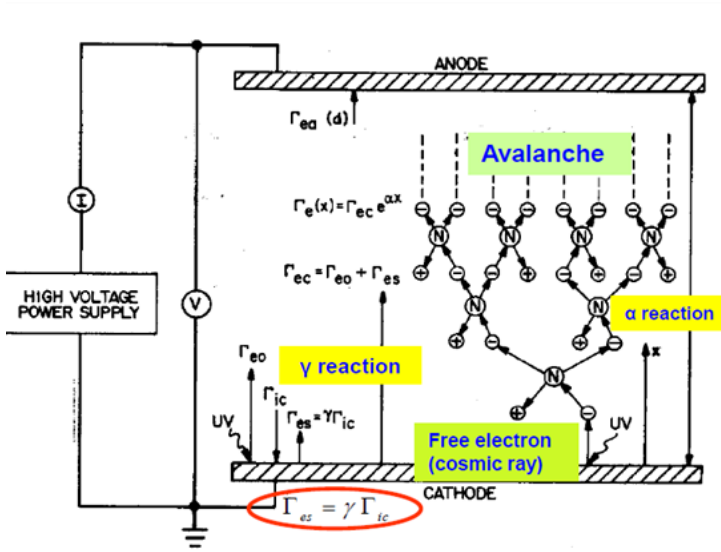

Figure 2.1 Schematic of a gas breakdown between a vacuum gap

2.1.1. α process

Townsend analyzed the phenomenon of electron-induced ionization amplification, utilizing the emitted photoelectrons when exposed to ultraviolet (UV) radiation and using them as seed electrons. By varying the intensity of UV radiation and controlling the initial electron current emitted from the cathode in the dark condition before discharge initiation, he measured a small current known as the dark current flowing to the anode. Townsend established the following relationship, denoted by (1).

$$\ln\left(\frac{I}{I_0}\right) \propto d \qquad (1)$$

In this equation, the proportionality constant is denoted as α and defined as the Townsend's first ionization coefficient of gas discharge. Using this coefficient, the first experimental formula of Townsend (2) is derived. This equation describes the exponential increase in discharge current caused by the charge entering the electrode as electrons are accelerated and move through the electric field.

$$I = I_0 \exp(\alpha d) \tag{2}$$

Townsend's second experimental formula (3) explains that the Townsend's first ionization coefficient depends on the operating pressure p and the strength of the electric field E. The experimental constants A and B in this equation vary based on the gas type and discharge regime (E/d), and representative values for these constants for different gas types are introduced in Table 2.1.

$$\frac{\alpha}{p} = A \exp\left(-\frac{B}{E/p}\right) \tag{3}$$

Gas	A (Torr cm^{-1})	B ($V(Torr\ cm)^{-1}$)	p/E ($V(Torr\ cm)^{-1}$)
He	3	34	$20-150$
Ne	4	100	$100-400$
Ar	12	180	$100-600$
Kr	17	240	$100-1000$
Xe	26	350	$200-800$
Hg	20	370	$150-600$
H2	5	130	$150-600$
N2	12	342	$100-600$
N2	8.8	275	$27-200$
Air	15	365	$100-800$
CO_2	20	466	$500-1000$
H_2O	13	290	$150-1000$

Table 2.1 Constants and ranges of applicability for (3), the ionization coefficient

2.1.2. γ process

Since the α effect requires seed electrons, plasma cannot be sustained solely by temporary seed electrons from cosmic rays or the photoelectric effect. Therefore, the emission of electrons from the surface, known as the γ effect, is necessary when the surface receives energy exceeding its work function through the collision of high-energy ions with a solid surface, the de-excitation reaction of metastable species, or the collision of photons. Townsend's second ionization coefficient, γ, is defined as the ratio of the emitted electron current to the ion current incident on the cathode, including electrons, ions, metastable atoms and molecules,

photons, and even fast neutrals. In general, for a 1D discharge, the effect of the ion-induced emissions is dominant so that it is expressed as (4).

$$\gamma = \frac{I_e}{I_i} \tag{4}$$

2.1.3. Paschen Curve

By utilizing the Townsend theory's α and γ process mentioned above, we can derive the breakdown voltage of a typical glow discharge. Let's consider the distance between the electrodes as d and the seed electron current generated by cosmic rays or the photoelectric effect as I_0. According to Equation (2), these seed electrons undergo collision ionization while being accelerated by the electric field, resulting in an increased current of $I_0 e^{\alpha d}$ when they reach the anode. Here, the ion current generated by ionization, excluding the initial current I_0, becomes $I_0(e^{\alpha d} - 1)$. These ions are accelerated towards the cathode by the electric field, allowing secondary electrons to be emitted from the cathode. According to (4), the current of these emitted secondary electrons becomes $\gamma I_0(e^{\alpha d} - 1)$. These secondary electrons then become seed electrons and repeat the same process, resulting in a continuous flow of current that sustains the discharge.

In a scenario where sufficient energy is supplied, we can assume a situation where ionization proliferation occurs infinitely due to the α and γ processes. As a

result, when we sum up the final current, it can be expressed in the form of an infinite geometric series, as shown below.

$$I = I_0 e^{\alpha d} + \eta I_0 e^{\alpha d} + \eta^2 I_0 e^{\alpha d} + \cdots = \frac{I_0 e^{\alpha d}}{1 - \eta} \tag{5}$$

When the variable $\eta = \gamma(e^{\alpha d} - 1)$ becomes 1, the denominator becomes zero, resulting in an infinitely large discharge current. Townsend defined this as the breakdown condition. By using this condition, we can derive Paschen's law for the breakdown voltage. By multiplying both sides of (5) by pd and substituting the breakdown condition of Townsend, we can calculate the breakdown voltage V_B.

$$V_B = V_B(pd) = \frac{Bpd}{\ln(Apd) / \ln\left(1 + \frac{1}{\gamma}\right)} \tag{6}$$

2.1.4. Gas breakdown model considering the space-charge distortion

As shown from the derivation above, conventional model of the gas discharge is independent of the initial current density, treating the electric field profile as uniform along the discharge. However, in fact, the ions produced by the electron impact ionizations are much heavier than the electrons so that local space charge is built up inside the gap. This space charge is usually very small that we could easily neglect, but as we deal with an irregular discharge with a background plasma, we constructed a revised model of gas breakdown, using the basic framework of the one-dimensional Townsend's model.

We the Poisson's equation (7) with the conventional Townsend's model. We assume drifting electrons and ions $v = \mu E$, assuming $\mu_e \gg \mu_i$. Unlike classical law, α should be considered as a function of electric field intensity, or the corresponding position. One can solve (7) numerically, to get the electric field profile distortion emerged from the space charge build-ups.

$$\frac{dE}{dx} = \frac{e}{\varepsilon_0}(n_i - n_e) = \frac{1}{\varepsilon_0 E}\left(\frac{j_i}{\mu_i} - \frac{j_e}{\mu_e}\right) = \frac{j_0}{\varepsilon_0 \mu_i E}\left(e^{\left(\int_0^d \alpha(E)dx\right)} - e^{\left(\int_0^x \alpha(E)dx\right)}\right) \tag{7}$$

After that, the total amount of the particle multiplication across the gap $\int_0^d \alpha(E)\, dx$ could be calculated and the breakdown voltage can be determined with the same treatment as the classical Townsend's model. Since the Townsend's first ionization coefficient is non-linearly proportional to the strength of the electric field, the distortion of the electric field profile results in the enhancement of total ionization even with the same applied voltage. Hence, the ignition of the gas discharge would be further eased if there is a sufficient amount of initial current j_0.

2.2. Secondary electron emission

Secondary electrons can be emitted through reactions with various entities such as the surface material, positive ions, metastable species, electrons, thermal energy, electric fields, and photons. Nevertheless, these mechanisms share a physical

background that could be explained in this section. Secondary electron emission from metal surfaces and positive ions was proposed by Penning in 1928. Figure 2.2 represents a schematic diagram illustrating the energy levels of electrons in the electrode and in space. The reference point is set at 0 V, indicating the bulk state of the space with respect to the potential in free space. The energy of the metal electrode consists of the conduction band, which is the energy range where free electrons exist in the metal, and the energy range corresponding to the work function (E_{Φ}), which is the energy required for electrons to escape from the metal and enter free space. The energy difference between the lowest energy level of the conduction band and the highest energy level corresponds to the Fermi energy (E_F).

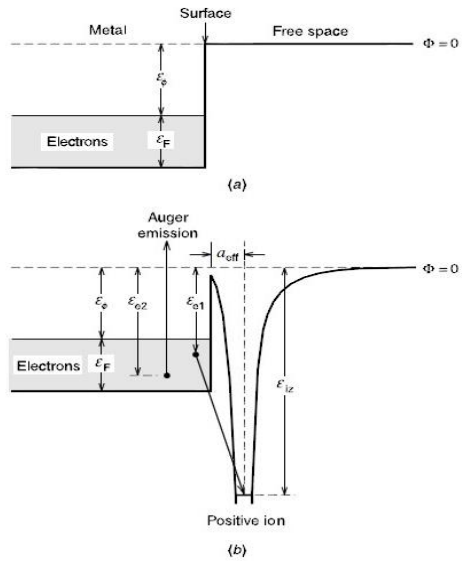

Figure 2.2 Schematic diagram illustrating the concepts of work function (E_Φ), Fermi energy (E_F), and Auger electron emission due to electron tunneling.

Positive ions incident on the cathode undergoes a tunneling effect, resulting in the emission of electrons from the cathode and causing ionization energy to be released through recombination reactions.

$$e^- + A^+ + S \rightarrow A + S + E_{iz} \qquad (6)$$

Here, A represents the incident atom, S represents the electrode surface, and E_{iz} denotes the ionization energy released through recombination reactions. In this context, the energy possessed by the participating electron within the metal is denoted as E_{el}. The net energy released through this reaction, known as the effective energy, can be expressed as shown in (7).

$$\Delta E = E_{iz} - E_{el} \quad (7)$$

The effective energy ΔE is utilized in two main types of reactions. The first reaction involves neutralizing the ionized particle to a metastable state. Through this reaction, the particle in the metastable state transitions to the ground state and emits recombination radiation. The second reaction is Auger neutralization. When an electron with energy E_{e2} receives recombination energy and is emitted, it is referred to as Auger emission, and the emitted electron is classified as a secondary electron. The conditions for Auger emission to occur can be expressed as $\Delta E > E_{e2}$, which predicts that the secondary electron emission coefficient due to ion collisions scales as $E_{iz} - 2E_{\Phi}$. If the collision energy of the ion is lower than keV, the secondary electron emission coefficient, γ, is determined solely by the type of electrode surface, its contamination level, and the gas species present. Raizer established an empirical formula for γ, which can be expressed as $\gamma_i = 0.016(E_{iz} - 2E_{\Phi})$. Based on the equation, the uncertainty in the calculated γ is known to be 50%. In this study, using argon gas and SUS304 electrodes, the value of γ under these conditions is approximately 0.15.

Chapter 3. Methods

3.1. Experimental setups

To investigate narrow hole breakdown, we designed a unique modular device (Figure 3.1) that facilitated controlled experiments. This device consists of an alumina block with a void hole measuring 1 mm in diameter and 10 mm in height, along with a stainless-steel block cathode biased negatively to manually induce gas breakdown. The narrow hole breakdown phenomena were studied both in the presence and absence of a background plasma formed underneath the modular device.

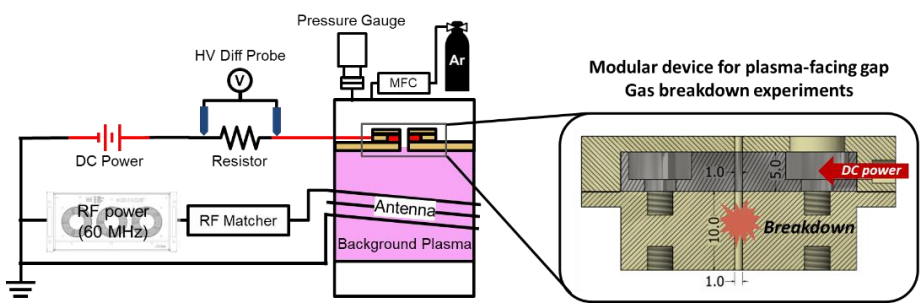

Figure 3.1 Inductively coupled plasma source and the modular device for plasma-facing narrow hole breakdown experiments.

In our experimental setup, a 60 MHz power was applied to a three-turn antenna coil through an automatically operated L-type matching network to ensure that the power reflection remained below 1%. The chamber naturally exhibits a pressure gradient due to limited gas flow caused by the narrow hole size. To address this, we attached an additional mass flow controller at the bottom of the chamber, enabling manual control of the pressure in the upper and lower regions of the chamber, respectively. By varying the gas pressure and the RF power, we were able to adjust the properties of the background plasma, as depicted in Figure 3.2. It is worth noting that the electron temperature was found to be insensitive to the operating conditions, whereas the electron density was proportional to the RF power. For our experiments, the Argon gas pressure in the bottom region was fixed at 40 mTorr.

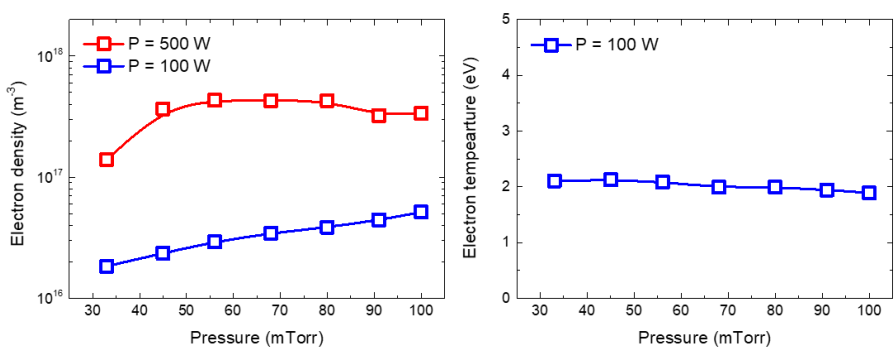

Figure 3.2 Electron density (m^{-3}) and temperature (eV) of the background plasma measured by an RF-compensated Langmuir Probe, differing the gas pressure and operating RF power.

Gas breakdown characteristics were analyzed by obtaining Paschen curves, which illustrate the relationship between breakdown voltages and gas pressures. To measure the plasma current, a safety resistor of 40 kΩ was placed between the DC power and the cathode, and a high-voltage differential probe was used. The breakdown voltage was determined as the DC power voltage just before the plasma current abruptly increased due to the avalanche effect. When a background plasma was present beneath the module, the plasma acted as an anode due to its positive plasma potential, which typically ranged from a few volts. Conversely, in the absence of background plasma, a grounded metal plate was attached to the bottom of the module to maintain a consistent voltage across the gap. To facilitate easy repetition of the breakdown experiments, we automated the system using LABVIEW. Figure 3.3 illustrates the appearance of gap breakdown in the presence of background plasma, depicted as a glow inside the narrow hole. The gap breakdown without background plasma exhibited a similar appearance, but its appearance not produced in this thesis.

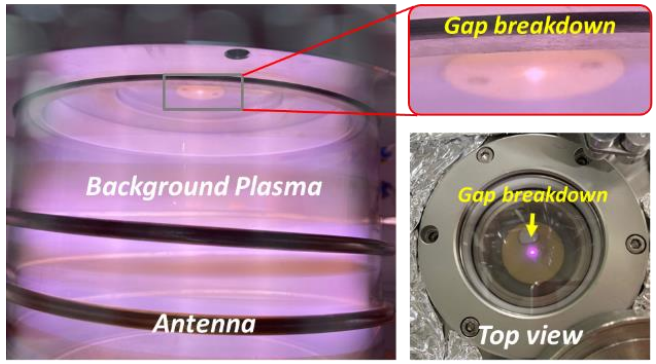

Figure 3.3 Appearance of an additional gas breakdown inside the narrow hole in the presence of the background plasma.

2.2. Simulation method

Since the gap size is very small, conventional assumptions of plasma fluid may not be valid on this problem. Hence, multi-dimensional kinetic simulations such as particle-in-cell (PIC) method must be secured for this problem. The PIC method is a numerical technique used to simulate the behavior of charged particles in a plasma or electromagnetic field. It is commonly employed in various fields of physics and engineering, including plasma physics, accelerator physics, and computational electromagnetics. The PIC method combines two key components: the discretization of space into a grid and the representation of particles as macro-particles. The simulation domain is divided into a grid of cells, and each cell serves as a discrete computational volume. The particles are approximated by assigning them to the cells based on their positions. The simulation proceeds in a time-stepping

manner. In each time step, the PIC method involves the following main steps: (1) Particle Push: The motion of individual particles is calculated using the equations of motion (typically Newton's laws) and electromagnetic interactions. The forces acting on the particles are determined based on the electric and magnetic fields present in the simulation domain. (2) Charge and Current Deposition: The macro-particles contribute their charge and current densities to the grid cells they occupy. This involves distributing the charge and current carried by each particle onto the nearby grid points. The charge deposition assigns a charge density to the grid cells, while the current deposition determines the current density. (3) Field Solve: The electromagnetic fields in the simulation domain are computed based on the charge and current densities on the grid. This step involves solving Maxwell's equations numerically, typically using finite-difference or finite-volume methods. The fields are calculated at each grid point. (4) Particle Interpolation: The electric and magnetic fields computed on the grid are interpolated back to the particle locations. This interpolation step provides the fields required for the particle push step in the next time step. If one wants to consider the collision between particles, both deterministic and probabilistic method could be applied. For example, Monte Carlo Collision (MCC) method is a well-known algorithm of probabilistic collision.

In this research, a 2D-3V PIC code, EDIPIC-2D (Electrostatic Direct Implicit Particle-In-Cell 2D), is utilized to study narrow hole breakdown considering various complexities. The particle dynamics is governed by acceleration inside the electric field and by collisions with the background gas, tracked with the MCC

technique. This code has been applied to many problems in non-local kinetics, discharges, and gas breakdowns of low-temperature plasma [69−75]. In the earlier 1D version, detailed instructions on the algorithms of the code are illustrated [69]. Constant value of the ion-induced secondary electron emission coefficient $\gamma_i = 0.15$ is assumed because most of the ions have energy lower than 1 keV [76−78]. Modified Vaughan's model is used to provide a continuum function the electron-induced secondary electron emission yield [79]. This model classifies the e-SEE into three reactions: elastic reflection, inelastic reflection, and true secondary emission with nine coefficients, and fitted to the experimentally measured SEE field, as elaborated in [69]. Argon is set to be the operating gas, and elastic collision, ionization, and excitation collisions are considered. The possible pressure gradient inside the narrow structure is neglected. The cell size $\Delta x = 5 \times 10^{-5}$ m and time step $\Delta t = 4$ ps are fine enough to capture the movement of electrons at the scale of Debye length corresponding to the increased density after the breakdown. The initial density of electrons and ions n_{init} was assumed to be 10^{14} m^{-3}, 0.1–1 % of the density at the steady state after the breakdown. Ten macro-particles per cell per species represent the initial charged-particle population.

Various types of gas breakdowns in narrow holes can be simplified as a simulation domain shown in Figure 3.4. It consists of a plasma container at the bottom region and a narrow hole along the y-axis, where background plasma generation and additional gas breakdown occurs, respectively. The red, gray, and black boxes correspond to the cathode, dielectric wall, and anode, respectively. The

surface material is set to be stainless steel for the anode and cathode and boron nitride for the dielectric wall. The e-SEE from the dielectric wall is treated as a function of the electron energy, as shown in Figure 3.5. In this code, the metal surface has an input potential, and the dielectric surface has a self-consistently determined floating potential. The metal surface boundary condition is implemented for the cathode and anode, while dielectric surface boundary condition is implemented for the dielectric wall. The y-axis is set as the symmetry.

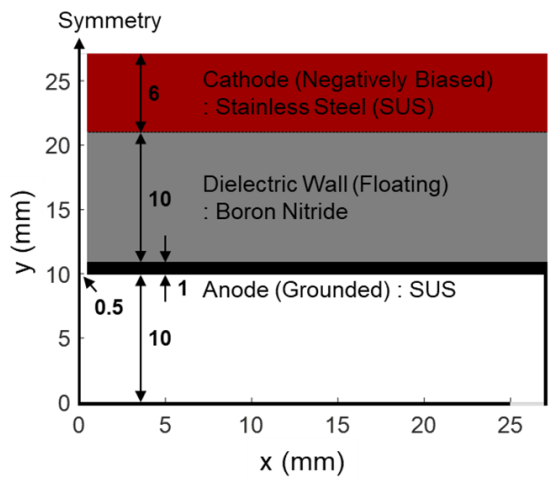

Figure 3.4 Simulation domain of narrow hole facing a plasma chamber. Red, gray, and black boxes or lines correspond to metal cathode, dielectric wall, and metal anode, respectively.

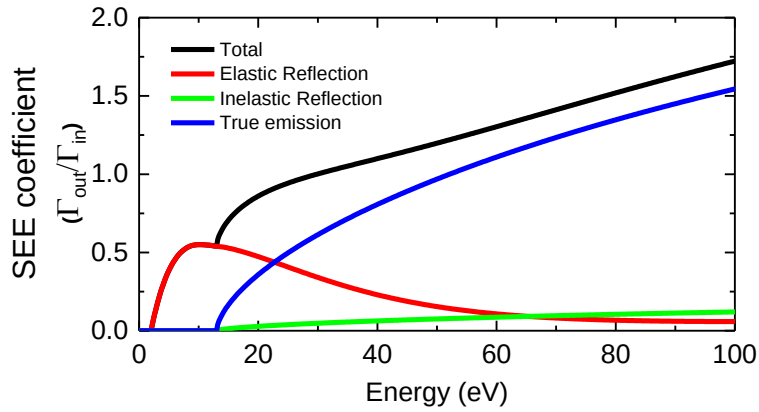

Figure 3.5 Electron induced secondary electron emission coefficient of boron nitride used for the simulation [69].

4. Fundamental mechanism of gas breakdown in narrow holes

4.1. Time evolution of narrow hole gas breakdowns

We run each of the simulations longer than 1μs to capture the development of the discharge and investigate the fundamental mechanism of the narrow hole gas breakdown. An example of the temporal evolution of plasma parameters is shown in Figure 4.1. Here, the pressure was set to 5 Torr, and the cathode was biased as $V_{hole} = -500$ V. We observe the localization of the potential drop near the cathode from the time evolution of potential structure in figure 4.1(c) (near $t = 25$ ns). From the charged particle distributions, we are convinced that the potential drop corresponds to the cathode sheath, since there forms a quasi-neutral region in front of the drop. As time flows, the discharge resembles a typical DC glow discharge with a cathode fall existence [76−78]. The electron density is on the core region of the narrow hole is higher than $n_e = 10^{17}$ m^{-3}, while the electron temperature T_e is about less than 3 eV and the plasma potential is about $V_p = 1.5\,V$. To investigate further, we studied how the two key process of the gas breakdown, α and γ, works in narrow hole gas breakdown.

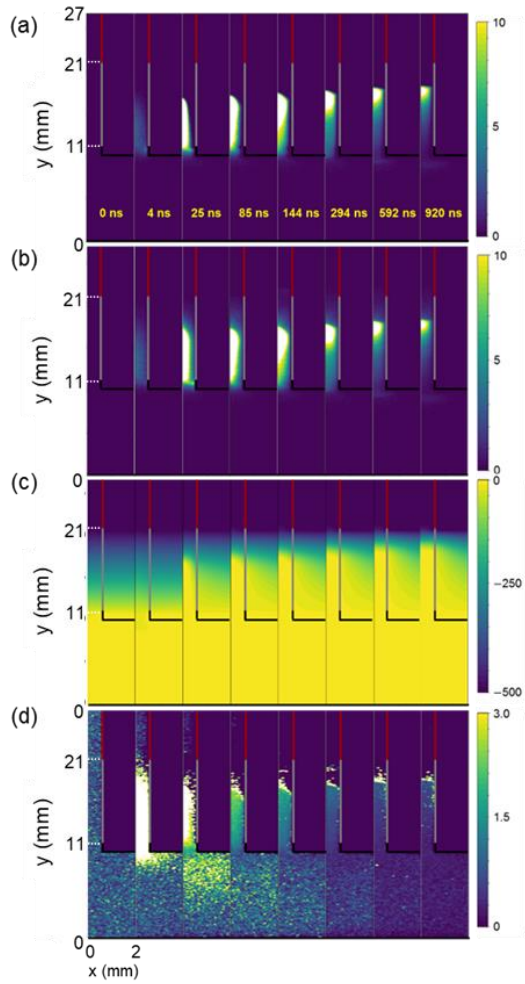

Figure 4.1 Temporal evolution of plasma parameters during the narrow hole breakdown; (a) the electron density ($\times 10^{16}$ m^{-3}), (b) the ion density ($\times 10^{16}$ m^{-3}), (c) potential (V), and (d) the electron temperature (eV). The red, gray, and black lines correspond to cathode, dielectric wall, and anode, respectively.

4.2. α process of narrow hole gas breakdowns

Volumetric ionization process, or α process, is studied by capturing the spatial particle density and electric field distributions that are linked to the particle multiplication. Tracking the change in particle density distribution by the time, we can clearly see the difference of whether the breakdown has occurred or not. Figure 4.2 is the contour plot of the temporal evolution of the electron density profile along the symmetric axis (x=0 mm) when we applied different V_{hole}. A transparent sheath and glow near the cathode can be observed when the breakdown occurs. In contrast, there is no electron avalanche or sheath when the breakdown does not occur.

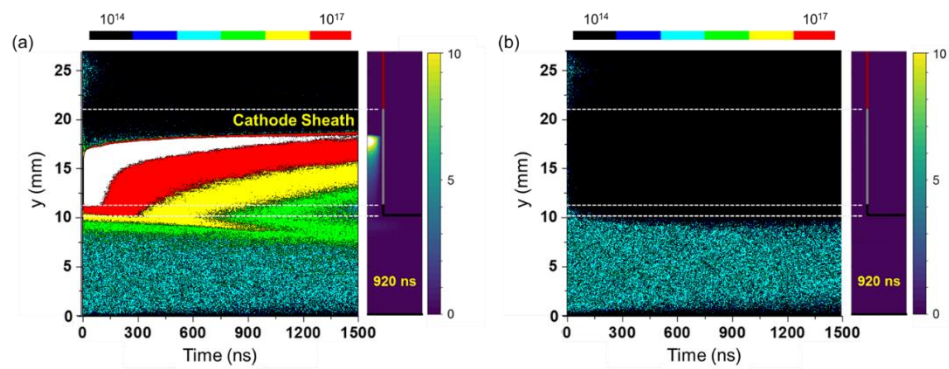

Figure 4.2 Contour of electron density (m^{-3}) along the symmetry axis (x=0 mm) versus time (ns). For the cases when the breakdown (a) occurs (V_{hole}=−500 V) and (b) does not (V_{hole}=−300 V). Contour plot of electron density is in logscale. Right side of each contours show the distribution of electron density ($\times 10^{16}$ m^{-3}) after the breakdown process.

As mentioned above, the cathode sheath is formed and the quasi-neutrality of charged particles is satisfied at t=25 ns. To see the governing physics of the breakdown, we focused on the earlier stage of breakdown, which is before t=25 ns. In Figure 4.3, temporal evolutions of charged particle density and axial electric field profile along the symmetric axis are presented. In case (a), where the breakdown occurs, a significant space-charge distortion near the cathode is seen during the initial electron avalanche. This non-neutral region localizes the electric field and enhances the field's strength, stimulating the α process. This contradicts the case (b), where the breakdown does not occur. Difference in the primary spatial multiplication of electrons during the travel from the cathode to the anode results in this distinction. The lack of initial avalanche fails to make sufficient space-charge distortion, so the uniform electric field between the cathode and anode does not change. The applied cathode voltage is no more than twice, but the nonlinear enhancement of electric field due to the space-charge distortion results in a significant difference in the dynamics of the discharge ignition. This is very similar to the volumetric ionization process to other types of typical gas discharges, so we can assume that the α process of a narrow hole breakdown is coherent the conventional knowledge [76-78].

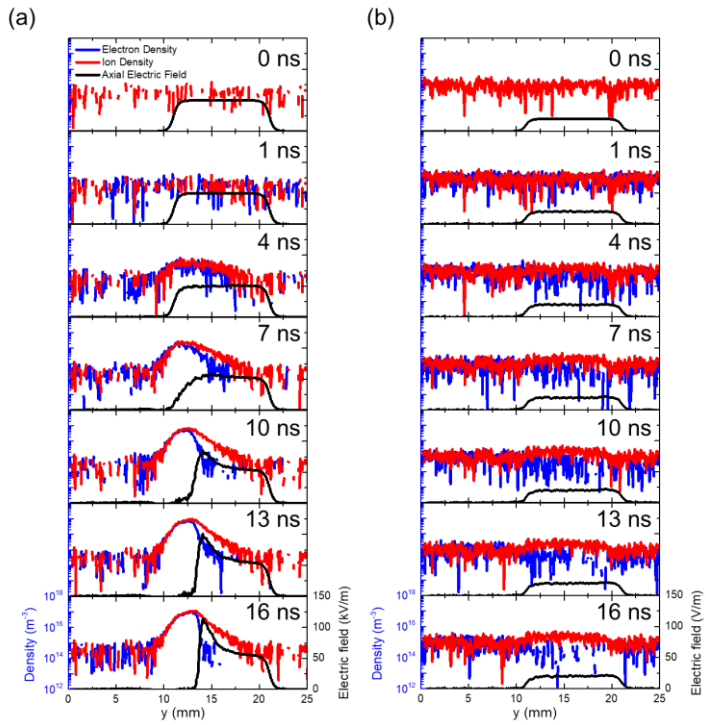

Figure 4.3 Temporal evolution of electron density (m^{-3}), ion density (m^{-3}), and axial electric field strength (V/m) profiles along the symmetric axis, when the breakdown (a) occurs ($V_{hole} = -500$ V) and (b) does not ($V_{hole} = -300$ V).

4.3. γ process of narrow hole gas breakdowns

The secondary electron emission process, also known as the γ process, is an important aspect of studying gas discharges. It involves capturing the fluxes of charged particles that collide with and emit from a surface. In conventional gas discharges, the ion-induced secondary electron emission from the cathode surface is considered to be the major source of secondary electrons, which play a crucial role in gas breakdown and discharge maintenance [76-78].

In Figure 4.4, the recorded particle fluxes at the cathode, radial dielectric wall, and anode are shown from the early stage of the breakdown until the steady discharge. The pressure in this case was set to 5 Torr, and the cathode was biased at $V_{hole} = -500\ V$. Unlike typical discharges, it is observed that not only the number of colliding particles but also the number of emitting electrons from the dielectric wall is the largest among all surfaces. This is attributed to the high aspect ratio of the narrow hole, which increases the likelihood of particles colliding with the radial wall. Previous studies have suggested that the colliding fluxes at the radial wall can increase with the aspect ratio [22-28], but the impact of the substantial number of emitted particles from this surface has not been thoroughly investigated.

These findings indicate that the emission of a significant number of particles from the dielectric wall in a narrow hole discharge can have a significant influence on the overall discharge dynamics. Understanding and quantifying these emission processes are crucial for comprehending the behavior of gas breakdown in

such geometries. Further research is needed to fully explore the implications of these particle fluxes and their effects on the discharge characteristics in narrow hole configurations.

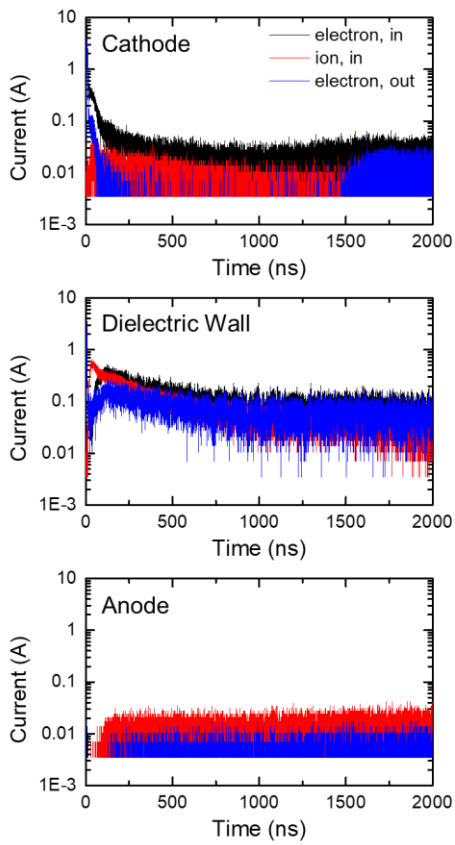

Figure 4.4 Temporal evolution of charged particle currents colliding and emitting from the surface when the pressure is set to 5 Torr and the cathode is biased as $V_{hole} = -500$ V.

Figure 4.5 depicts the normalized intensity of electrons colliding with each surface as a function of their energy. The plot indicates that the radial flux of electrons primarily consists of particles with relatively low energies. These low-energy electrons are more likely to undergo elastic reflections at the dielectric wall, as mentioned earlier. This observation suggests that in high aspect ratio narrow hole breakdowns, the electron-induced secondary electron emission, particularly electron scattering, plays a significant role.

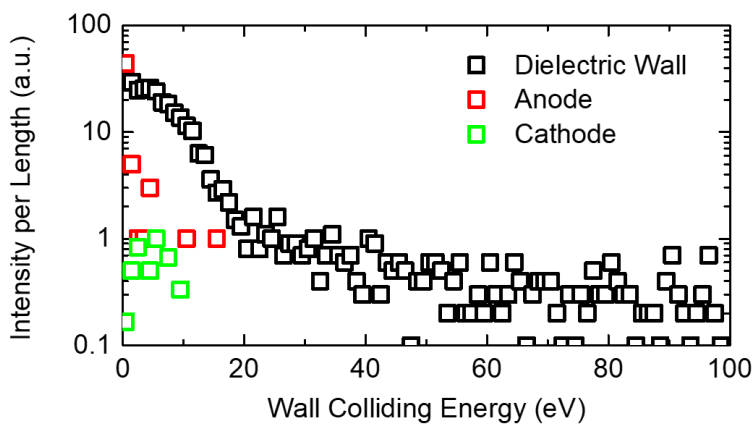

Figure 4.5 Normalized electron energy distribution colliding at each surface measured at $t = 100$ ns. Amounts of colliding particles at certain energy intervals are divided by the colliding surface's length.

To quantitatively analyze the importance of each secondary electron emission reaction, we conducted simulations by selectively disabling each reaction

in the simulation code. The increase in the breakdown voltage was measured for each case. Figure 4.6 illustrates the results obtained. It is observed that when the elastic reflection from the dielectric wall is turned off, the breakdown voltage exhibits the highest increase. This outcome aligns with the expectations based on the electron energy distribution function discussed earlier.

Similar analyses were conducted for wider diameter holes, revealing that the significance of the wall condition, particularly the electron-induced secondary electron emission, is much greater in narrower gaps. Hence, when investigating narrow holes, it is crucial to thoroughly consider the effects of electron-induced secondary electron emission. These findings emphasize the importance of accurately accounting for the electron-induced secondary electron emission and its impact on gas breakdown in narrow holes. This information is valuable for developing a comprehensive understanding of the breakdown characteristics in such systems.

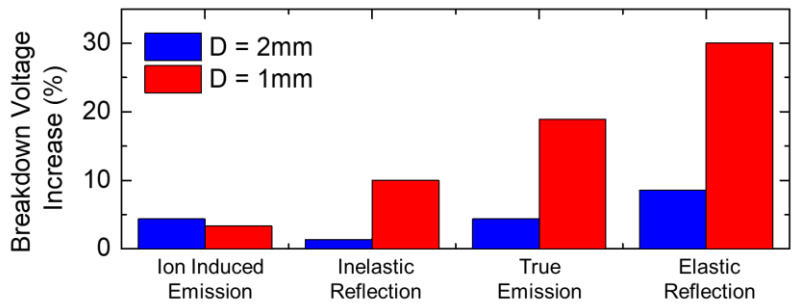

Figure 4.6 Breakdown voltages differing the secondary electron emission properties of the dielectric wall, for a wider (D = 2 mm) and a narrower (D = 1 mm) hole. Each of the bars represent the increment of the voltage when turned each of the reactions off.

Chapter 5. Role of background plasma on narrow hole gas breakdowns

5.1. Experimental observation of undervoltage breakdowns

In order to comprehensively investigate the effect of background plasma on narrow hole gas breakdown, a series of experiments were conducted. The obtained Paschen curves, presented in Figure 5.1, revealed a significant reduction in breakdown voltages when background plasma was present. The y-axis in the figure represents the cathode potential, with the assumption that the anode potential is zero due to the negligible potential of the background plasma. Although the plasma can function as a positively biased anode, resulting in a slight shift in the curve by a few volts, the actual reduction in breakdown voltage due to background plasma was found to be on the order of hundreds of volts. This finding indicates that the role of background plasma is not limited to that of a simple positive anode, and it has a much more substantial impact on gas breakdown. The abrupt voltage drop depicted in the curves further clarifies the origin of unintended breakdowns in processing plasma sources, highlighting the importance of considering steady-state background plasma as a significant factor in such cases.

These experimental results provide quantitative evidence of the influence of background plasma on narrow hole gas breakdown, underscoring the need to account for the presence and characteristics of background plasma when studying and addressing unintended breakdown phenomena in processing plasma sources. In practical processing applications, surface charging resulting from charged particle collisions or exposure to high voltages is comparable to the manually biased cathode in our experiments, serving as the source of energy for electrons. Therefore, our findings can be useful in providing a better understanding of the fundamental mechanisms involved in gas breakdown in narrow holes, facilitating the design and optimization of processing plasma sources.

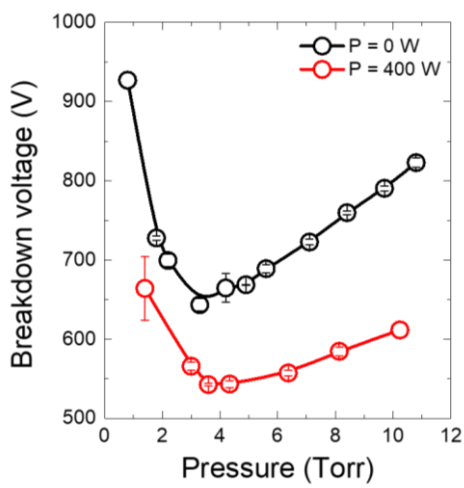

Figure 5.1 Experimentally obtained Paschen curves in the absence (black, RF power P = 0 W) and presence (red, P = 400 W) of the background plasma.

After obtaining the Paschen curves, we conducted additional experiments by deliberately damaging the gap surface through dozens of gap discharges. This allowed us to simulate the conditions encountered in industrial plasma processes. Figure 5.2(a) presents the results, which demonstrate a further decrease in breakdown voltages compared to the previous experiments. We hypothesize that the damage to the gap surface has a significant impact on the gas breakdown process. To investigate this hypothesis, we measured the surface roughness and discovered that frequent gap breakdowns can permanently deform the surface, as depicted in Figure 5.2(b), leading to increased roughness. We believe that this change in roughness contributes to the additional decline in the Paschen curves. As the surface becomes rougher, electron field emission from the surface may intensify, thereby promoting breakdown occurrences at lower discharge voltages. These findings suggest the existence of a positive feedback loop that operates to reduce the breakdown voltage in the presence of background plasma, which initiates this loop. However, a more comprehensive analysis of this voltage decrease should be pursued in future investigations. The observations from these experiments highlight the complex interplay between background plasma, surface damage, and surface roughness in narrow hole gas breakdown. Understanding and characterizing these phenomena are crucial for developing strategies to mitigate breakdown-related issues in practical plasma processes.

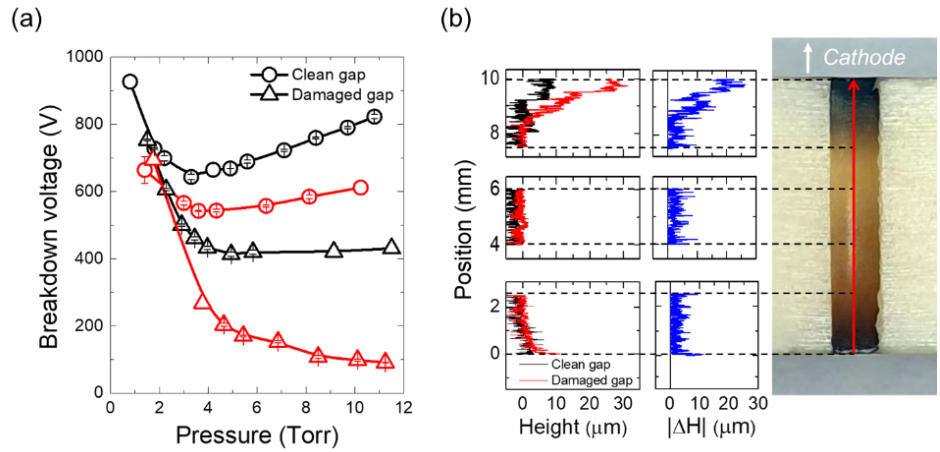

Figure 5.2 Experimentally obtained Paschen curves (a) before (circle) and after (triangle) the gap damages. (b) Gap surface roughness in the indicated area.

5.2. Kinetic simulation on the background plasma effect

In order to investigate the role of background plasma in the decrease of narrow hole gas breakdown voltages, a series of kinetic simulations were conducted. Figure 5.3(a) presents the Paschen curves obtained from the simulations, where the background plasma density was set to $10^{16}\ m^{-3}$. It should be noted that due to the limitations of our Cartesian 2D coordinate simulation, the actual magnitude of the breakdown voltage may differ from that observed in experiments using a cylindrical module. Nonetheless, despite this limitation, the simulations effectively captured the observed decrease in breakdown voltage caused by the presence of background plasma.

To understand the cause of this reduction, we monitored the charged particle density and local electric field within the gap. Figure 5.3(b) illustrates the time evolution of the density and electric field profile inside the gap, where the cathode potential was set to -300 V at 5 Torr. Our observations revealed that breakdown occurred only in the presence of background plasma, accompanied by a significant increase in the local electric field.

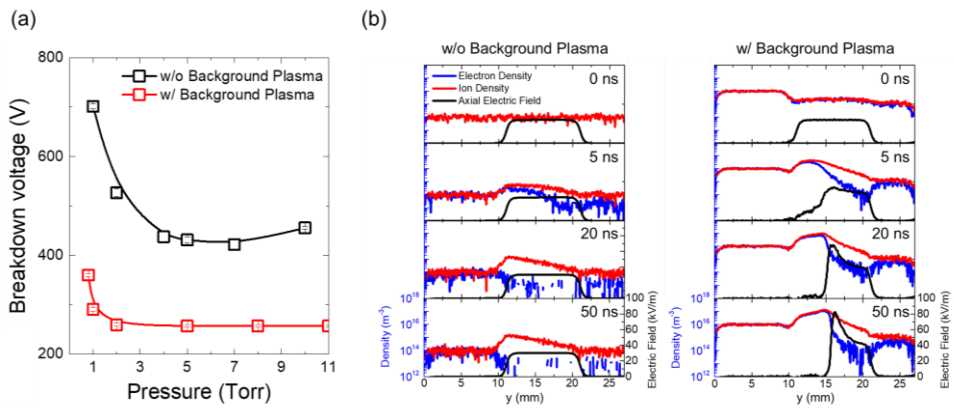

Figure 5.3 Kinetic simulation results: (a) Paschen curves without (black) and with (red) background plasma. (b) Time evolution of the electron density (blue), ion density (red) and electric field strength (black) profile inside the gap.

As mentioned in Chapter 2, the electric field profile, denoted as E, deviates from a uniform profile, while the total voltage across the gap, V, remains constant ($\int E\,dy$). According to the Gauss equation $\nabla \cdot E = \rho/\varepsilon_0$, any deviation from a

uniform profile can be attributed to the presence of space charge in the gap. The diffusion of particles from the background plasma leads to an initial current at the cathode, denoted as j_0, as ions within the gap accelerate towards the cathode and create secondary electrons. With an increase in j_0, the number of ions generated by the volumetric electron avalanche process also increases. Due to the heavier mass of ions compared to electrons, their presence results in an increased local space charge that distorts the electric field from a uniform profile $E(y) = E_0$ to a distorted profile $\tilde{E}(y) = E_0 + E_1(y)$, where $E_1(y)$ represents the amount of field distortion such that $\int_0^d E_1(y)\, dy = 0$. Since the Townsend ionization coefficient, α is nonlinearly proportional to the electric field strength, an increase in electric field caused by the distorted field profile leads to a higher total amount of ionization across the gap. The modified Townsend discharge model introduced in Chapter 2, is compatible to this explanation. For example, in the context of the Townsend ionization coefficient α expressed as $\alpha = kE^2$ [81], the total amount of ionization across the gap can be represented as $\mathrm{M} = \int_0^{\mathrm{d}} \mathrm{k}\tilde{E}^2\, \mathrm{dy} = \int_0^{\mathrm{d}} \mathrm{kE}_0^2\, \mathrm{dy} + \int_0^{\mathrm{d}} \mathrm{kE}_1^2\, \mathrm{dy}$. In this expression, the first term on the right-hand side corresponds to the total ionization in the case of a uniform electric field. This analysis highlights that the decrease in breakdown voltage observed in the presence of background plasma is primarily attributed to the particle flux originating from the plasma.

For further investigation, we implemented the results from the modified discharge model, running several more simulations in parallel. In detail, by solving

(7) by different initial conditions given as charged particle density, we could get the electric field distribution across the gap. Then, the multiplication factor M, which is the integral of α along the discharge column, is calculated using BOLSIG+ code. The breakdown voltages can be obtained by iterative calculations for different voltages using the one-dimensional gas breakdown criterion $M = 1 + 1/\gamma_i$, as shown in Figure 5.4(a). Compared to the Townsend model with zero initial density assumption, the space-charge distorted model strongly depends on increasing the initial density. Especially, the breakdown voltage is decreased by enlarging the initial particle number. Simulation results shown in Figure 5.4(b) shows distorted electric field profiles with varying the initial particle density from $10^{13}\ m^{-3}$ to $10^{15}\ m^{-3}$. As the profile of electric field squeezes, the local field magnitude increases, resulting in a larger multiplication, as shown in Figure 5.4(c). Even if the applied voltage of the hole cathode is the same, an increment of initial particle density stimulates the entire α process; finally, the breakdown voltage decreases. In Figure 5.4(d), we compared the results of PIC simulation and the space-charge distortion model. Due to the geometric simplification, the theory does not give the same value as simulation. Nevertheless, our space-charge distortion model successfully demonstrates the decreasing nature of breakdown voltage, which cannot be explained with discharge models assuming zero initial particle density.

Therefore, it becomes evident that blocking these particles from reaching the gap is a crucial factor in preventing unintended breakdown. By mitigating or

controlling the particle flux from the background plasma, it is possible to maintain a higher breakdown voltage and improve the stability of the system.

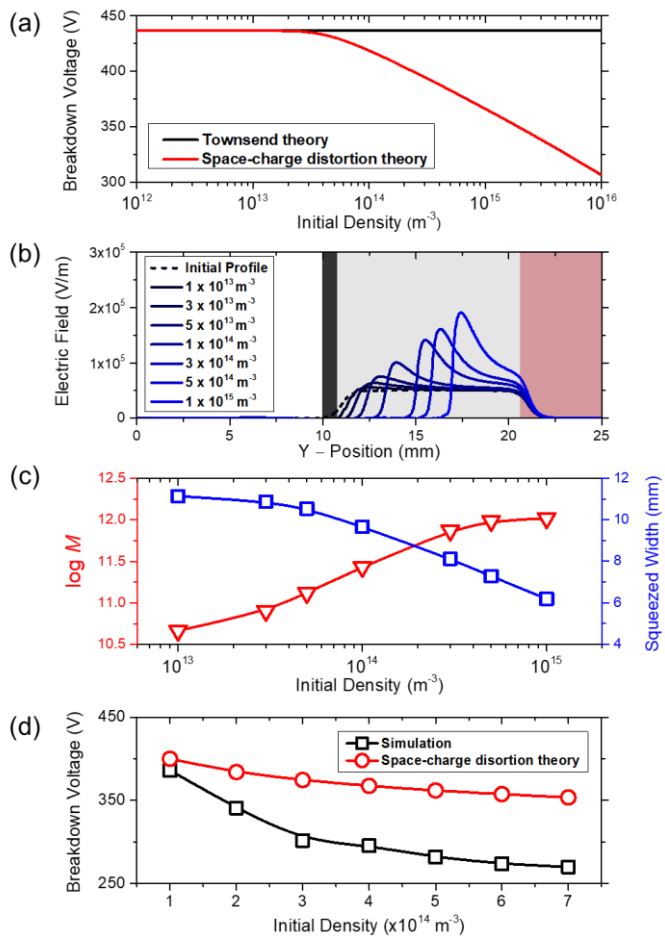

Figure 5.4 (a) Comparison of Townsend and the space-charge distortion model, (b) Electric field intensity profiles, (c) multiplication factor logM and squeezed width of the electric field profiles, and (d) breakdown voltages varying the initial particle density.

Chapter 6. Conclusions

In this study, we have undertaken a comprehensive investigation into the fundamental physics of gas breakdown inside narrow holes, utilizing two-dimensional kinetic simulations. Our research has shed light on the alpha and gamma processes involved in narrow hole breakdowns, highlighting the role of secondary electron emissions from the radial walls, particularly in structures with high aspect ratios. Furthermore, we have examined the influence of background plasma on these discharges.

A significant contribution of our work lies in unraveling the physics behind unintended breakdowns, which present considerable risks in advanced plasma sources employed in semiconductor fabrication. Through innovative experiments, we have quantitatively measured these breakdowns and observed a sharp decline in the Paschen curve when background plasma is present. Our kinetic simulations have validated these experimental observations, identifying particle influxes from the background plasma as the primary cause of this phenomenon. As the initial current intensifies, the electron avalanche becomes more pronounced, leading to the accumulation of local space charge, alteration of the electric field profile, and heightened total ionization. The consistent results obtained from both experiments and simulations indicate that unintended breakdowns can be mitigated by effectively blocking particle fluxes originating from the plasma. This insight serves as a catalyst

for further research endeavors focused on comprehending charged particle transport in complex processing plasmas and developing methods to shield particle fluxes, such as through the modification of gap structures or the application of magnetic fields.

By advancing our understanding of the underlying physics governing gas breakdown in narrow holes and proposing strategies to prevent unintended breakdowns, this study makes valuable contributions to the enhancement of plasma sources used in semiconductor manufacturing and other related applications. The findings and insights obtained pave the way for the development of more reliable and efficient plasma processes, ultimately benefiting the semiconductor industry and contributing to technological advancements in various fields.

Bibliography

[1] F. Paschen, Ueber die zum funkenübergang in luft: wasserstoff und kohlensäure bei verschiedenen drucken erforderliche potentialdifferenz. (JA Barth, 1889).

[2] J. S. Townsend, Electricity in gases. (Рипол Классик, 1915).

[3] A. Von Engel and L. Marton, Physics Today 18 (10), 64 (1965).

[4] Y. P. Raizer and J. E. Allen, Gas discharge physics. (Springer, 1991).

[5] G. Carter and J. S. Colligon, AMERICAN ELSEVIER PUBLISHING CO., NEW YORK, 1968. 446 P (1968).

[6] K. H. Krebs, Fortschritte der Physik 16 (8), 419-490 (1968).

[7] J. Townsend and S. MacCallum, The London, Edinburgh, and Dublin Philosophical Magazine and Journal of Science 6 (38), 857-878 (1928).

[8] S. McCallum and L. Klatzow, The London, Edinburgh, and Dublin Philosophical Magazine and Journal of Science 17 (111), 291-297 (1934).

[9] H. C. MILLER, INTERNATIONAL JOURNAL OF ELECTRONICS 22 (1), 31-34 (1967).

[10] J. Y. Kim, I. Kaganovich and H.-C. Lee, Plasma Sources Science and Technology 31 (3), 033001 (2022).

[11] H. Conrads and M. Schmidt, Plasma Sources Science and Technology 9 (4), 441 (2000).

[12] H.-C. Lee, Applied Physics Reviews 5 (1), 011108 (2018).

[13] V. Lisovskiy, S. Martins, K. Landry, D. Douai, J.-P. Booth, V. Cassagne and V. Yegorenkov, Physics of Plasmas 12 (9), 093505 (2005).

[14] V. Lisovskiy and V. Yegorenkov, Journal of Physics D: Applied Physics 31 (23), 3349 (1998).

[15] M.-G. Yoo, J. Lee, Y.-G. Kim, J. Kim, F. Maviglia, A. C. Sips, H.-T. Kim, T. S. Hahm, Y.-S. Hwang and H. J. Lee, Nature communications 9 (1), 1-13 (2018).

[16] K. Takahashi, Reviews of Modern Plasma Physics 3 (1), 1-61 (2019).

[17] J. Y. Kim, J. Y. Jang, J. Choi, J.-i. Wang, W. I. Jeong, M. Elgarhy, G. Go, K.-J. Chung and Y. Hwang, Plasma Sources Science and Technology 30 (2), 025011 (2021).

[18] A. Mishra, P. Kelly and J. Bradley, Plasma Sources Science and Technology 19 (4), 045014 (2010).

[19] S.-Z. Li and H. S. Uhm, Physics of plasmas 11 (7), 3443-3448 (2004).

[20] M. Radmilovic-Radjenovic and B. Radjenovic, IEEE transactions on plasma science 35 (5), 1223-1228 (2007).

[21] D. B. Go and D. A. Pohlman, Journal of Applied physics 107 (10), 103303 (2010).

[22] V. Lisovskiy and S. Yakovin, Technical Physics 45 (6), 727-731 (2000).

[23] V. Lisovskiy and S. Yakovin, Plasma Physics Reports 26 (12), 1066-1075 (2000).

[24] V. Lisovsky and S. Yakovin, Journal of Experimental and Theoretical Physics Letters 72 (2), 34-37 (2000).

[25] E. Bogdanov, S. Adams, V. Demidov, A. Kudryavtsev and J. Williamson, Physics of Plasmas 17 (10), 103502 (2010).

[26] V. Lisovskiy, S. Yakovin and V. Yegorenkov, Journal of Physics D: Applied Physics 33 (21), 2722 (2000).

[27] V. Lisovskiy, V. Koval and V. Yegorenkov, Physics Letters A 375 (19), 1986-1989 (2011).

[28] V. Lisovskiy, K. Artushenko and V. Yegorenkov, Physics of Plasmas 24 (5), 053501 (2017).

[29] Y. Li and D. B. Go, Journal of Applied Physics 116 (10), 103306 (2014).

[30] R. Tirumala and D. B. Go, Applied Physics Letters 97 (15), 151502 (2010).

[31] P. Rumbach and D. B. Go, Journal of Applied Physics 112 (10), 103302 (2012).

[32] A. Venkattraman and A. A. Alexeenko, Physics of plasmas 19 (12), 123515 (2012).

[33] W. Zhang, T. Fisher and S. Garimella, Journal of applied physics 96 (11), 6066-6072 (2004).

[34] M. Radmilovic-Radjenovic and B. Radjenovic, IEEE transactions on plasma science 35 (5), 1223-1228 (2007).

[35] M. A. Bilici, J. R. Haase, C. R. Boyle, D. B. Go and R. M. Sankaran, Journal of Applied Physics 119 (22), 223301 (2016).

[36] G. Meng, X. Gao, A. M. Loveless, C. Dong, D. Zhang, K. Wang, B. Zhu, Y. Cheng and A. L. Garner, Physics of Plasmas 25 (8), 082116 (2018).

[37] G. Meng, Q. Ying, A. M. Loveless, F. Wu, K. Wang, Y. Fu, A. L. Garner and Y. Cheng, Physics of Plasmas 26 (1), 014506 (2019).

[38] A. M. Loveless, G. Meng, Q. Ying, F. Wu, K. Wang, Y. Cheng and A. L. Garner, Scientific reports 9 (1), 1-7 (2019).

[39] R. S. Brayfield, A. J. Fairbanks, A. M. Loveless, S. Gao, A. Dhanabal, W. Li, C. Darr, W. Wu and A. L. Garner, Journal of Applied Physics 125 (20), 203302 (2019).

[40] D. Maric, N. Skoro, P. Maguie, C. Mahony, G. Malovic and Z. Petrovic, Plasma Sources Sci. Technol. 21, 035016-035011-035016 (2012).

[41] A. M. Loveless, A. M. Darr and A. L. Garner, Physics of Plasmas 28 (4), 042110 (2021).

[42] Q. Sun, Q.-h. Zhou, W. Yang, Y. Dong, H.-t. Zhang, M.-m. Song and Y. Wu, Plasma Sources Science and Technology 30 (4), 045001 (2021).

[43] Y. Fu, P. Zhang, J. Verboncoeur and X. Wang.

[44] A. L. Garner, A. M. Loveless, J. N. Dahal and A. Venkattraman, IEEE Transactions on Plasma Science 48 (4), 808-824 (2020).

[45] A. L. Garner, G. Meng, Y. Fu, A. M. Loveless, R. S. Brayfield and A. M. Darr, Journal of Applied Physics 128 (21), 210903 (2020).

[46] A. M. Loveless and A. L. Garner, Physics of Plasmas 24 (11), 113522 (2017).

[47] H. Berry, Physical Review 74 (7), 848 (1948).

[48] S. Ghosh and S. Khare, Physical Review 125 (4), 1254 (1962).

[49] J. R. M. Vaughan, IEEE Transactions on Electron Devices 36 (9), 1963-1967 (1989).

[50] A. Derzsi, I. Korolov, E. Schüngel, Z. Donkó and J. Schulze, Plasma Sources Science and Technology 24 (3), 034002 (2015).

[51] V. Lisovskiy, J.-P. Booth, K. Landry, D. Douai, V. Cassagne and V. Yegorenkov, Europhysics Letters 82 (1), 15001 (2008).

[52] I. Korolov and Z. Donkó, Physics of Plasmas 22 (9), 093501 (2015).

[53] M. U. Lee, J. Lee, J. K. Lee and G. S. Yun, Plasma Sources Science and Technology 26 (3), 034003 (2017).

[54] M. Radmilovic-Radjenovic and B. Radjenovic, IEEE transactions on plasma science 35 (5), 1223-1228 (2007).

[55] A. M. Loveless and A. L. Garner, Physics of Plasmas 24 (10), 104501 (2017).

[56] L. D. Tsendin, Physics-Uspekhi 53 (2), 133 (2010).

[57] H.-C. Lee, J.-K. Lee and C.-W. Chung, Physics of Plasmas 17 (3), 033506 (2010).

[58] H.-C. Lee, D.-H. Kim and C.-W. Chung, Applied Physics Letters 102 (23), 234104 (2013).

[59] Y. Fu, B. Zheng, P. Zhang, Q. H. Fan, J. P. Verboncoeur and X. Wang, Physics of Plasmas 27 (11), 113501 (2020).

[60] Y. Fu, B. Zheng, D.-Q. Wen, P. Zhang, Q. H. Fan and J. P. Verboncoeur, Applied Physics Letters 117 (20), 204101 (2020).

[61] A. Semnani, A. Venkattraman, A. A. Alexeenko and D. Peroulis, Applied Physics Letters 103 (6), 063102 (2013).

[62] M. Merola, D. Loesser, A. Martin, P. Chappuis, R. Mitteau, V. Komarov, R. Pitts, S. Gicquel, V. Barabash and L. Giancarli, Fusion Engineering and Design 85 (10-12), 2312-2322 (2010).

[63] K. Krieger, W. Jacob, D. Rudakov, R. Bastasz, G. Federici, A. Litnovsky, H. Maier, V. Rohde, G. Strohmayer and W. West, Journal of nuclear materials 363, 870-876 (2007).

[64] N. Y. Babaeva and M. J. Kushner, Journal of applied physics 101 (11), 113307 (2007).

[65] J. Park, Y. An, B. Jung, J. Lee, H. Lee, K.-J. Chung, Y.-S. Na and Y. Hwang, Fusion Engineering and Design 96, 269-273 (2015).

[66] J. Y. Park, J. Y. Kim, S. Kim, E. Jung and Y. Hwang, Physics of Plasmas 29 (5), 052112 (2022).

[67] P. Shi, P. Srivastav, C. Beatty, R. John, M. Lazo, J. McKee, J. McLaughlin, M. Moran, M. Paul and E. E. Scime, Physics of Plasmas 28 (3), 032101 (2021).

[68] L. Chen and L. Xu, (Google Patents, 2010).

[69] D. Sydorenko, Particle-in-cell simulations of electron dynamics in low pressure discharges with magnetic fields. (University of Saskatoon, 2006).

[70] D. Sydorenko, I. Kaganovich, Y. Raitses and A. Smolyakov, Physical review letters 103 (14), 145004 (2009).

[71] J. Carlsson, A. Khrabrov, I. Kaganovich, T. Sommerer and D. Keating, Plasma Sources Science and Technology 26 (1), 014003 (2016).

[72] S. Sharma, S. Patil, S. Sengupta, A. Sen, A. Khrabrov and I. Kaganovich, Physics of Plasmas 29 (6), 063501 (2022).

[73] H. Sun, J. Chen, I. D. Kaganovich, A. Khrabrov and D. Sydorenko, Physical Review Letters 129 (12), 125001 (2022).

[74] B. Jin, J. Chen, A. V. Khrabrov, Z. Wang and L. Xu, Plasma Sources Science and Technology 31 (11), 115015 (2022).

[75] L. Xu, A. V. Khrabrov, I. D. Kaganovich and T. J. Sommerer, Physics of Plasmas 24 (9), 093511 (2017).

[76] M. A. Lieberman and A. J. Lichtenberg, Principles of plasma discharges and materials processing. (John Wiley & Sons, 2005).

[77] Y. P. Raizer and J. E. Allen, Gas discharge physics. (Springer, 1991).

[78] P. Chabert and N. Braithwaite, Physics of radio-frequency plasmas. (Cambridge University Press, 2011).

[79] R. Vaughan, IEEE Transactions on Electron Devices 40 (4), 830 (1993).

[80] G. Hagelaar and L. C. Pitchford, Plasma sources science and technology 14 (4), 722 (2005).

[81] R. Varney, H. White, L. Loeb and D. Posin, Physical Review 48 (10), 818 (1935).

초 록

오랜 역사 속에서 연구되어 온 기체 방전은 플라즈마 물리학을 이해하는 것에 있어 가장 기초적인 지식이지만, 현실 속 다양한 상황에서의 복잡한 방전을 이해하는 것은 여전히 어려운 과제이다. 대표적으로, 좁은 홀 구조물에서의 기체 방전 현상을 이해하는 것은 배경 플라즈마가 존재하는 반도체 제조 장치에서의 의도하지 않은 아킹 현상을 해소하는 것에 있어 필수적이다. 본 연구에서는 제어된 실험환경을 구축하고, 2차원 플라즈마 동역학 시뮬레이션을 결합해 높은 종횡비를 가진 좁은 홀 구조에서의 기체 방전의 기초 물리학을 복합적으로 연구하였다. 결과 중 하나로, 좁은 구조물에서는 이차전자의 주요 공급원이 음극에서의 이온 유도 방출이 아닌 벽면에서의 전자 유도 방출이 됨을 확인하였다. 또한, 좁은 구멍 근처에 배경 플라즈마가 존재하는 상황을 모사해, 이 때 방전 전압이 크게 감소하여 의도하지 않은 방전이 쉽게 발생할 수 있음을 실험과 동역학 시뮬레이션에서 모두 확인하였다. 시뮬레이션 연구를 통해, 배경 플라즈마에서 홀 내부로 유입되는 하전 입자들에 의한 초기 전자 사태 과정이 홀 내부의 공간 전하 축적에 기여하여 전기장의 왜곡을 유발한다는 것을 확인하였다. 기체 방전의 이온화 계수는 전기장 세기에 비선형적으로 비례하므로, 이렇게 왜곡된 전기장 분포는 낮은 인가 전압에서도 높은 전자 증배를 유도해 방전 전압을 낮출 수 있음을 확인하였다.

Keyword: 기체 방전, 동역학 시뮬레이션, 입자-셀 방법 (Particle-In-Cell), 배경 플라즈마, 공간 전하, 플라즈마 공정

Student Number: 2020-24257